ACS OMEGA

http://pubs.acs.org/journal/acsodf

Article

Computational Study of the Thermal Rectification Properties of a Graphene-Based Nanostructure

Junjie Chen* and Lingyu Meng

Cite This: *ACS Omega* 2022, 7, 28030−28040

Read Online

ACCESS | Metrics & More | Article Recommendations

ABSTRACT: Thermally rectifying materials would have important implications for thermal management, thermal circuits, and the field of phononics in general. Graphene-based nanostructures have very high intrinsic thermal conductance, but they normally display no thermal rectification effects. The present study relates to a thermally rectifying material and, more particularly, to a graphene-based nanomaterial for controlling heat flux and the associated method determining the rectification coefficient. Thermal rectifiers using a graphene-based nanostructure as thermal conductors were designed. Vacancy defects were introduced into one end of the nanostructure to produce an axially non-uniform mass distribution. Modified Monte Carlo methods were used to investigate the effects of defect size and shape, vacancy concentration, and ribbon length on the thermal rectification properties. Anharmonic lattice dynamics calculations were carried out to obtain the frequency-dependent phonon properties. The results indicated that the nanoscale system conducts heat asymmetrically, with a maximum available rectification coefficient of about 70%. Thermal rectification has been achieved, and the difference in temperature dependence of thermal conductivity is responsible for the phenomenon. Defects can be tailored to modulate the temperature dependence of thermal conductivity. The power-law exponent can be negative or positive, depending upon the ribbon length and vacancy concentration. A computational method has been developed, whereby the numerous variables used to determine the rectification coefficient can be summarized by two parameters: the power-law exponent and the thermal resistance ratio. Accordingly, the rectification coefficient can be obtained by solving a simple algebraic expression. There are several structure factors that cause noticeable effects on the thermal rectification properties. Defect size, vacancy concentration, and ribbon length can affect the thermal conductance of the nanostructure symmetrically and significantly. Graphene-based nanostructure thermal rectifiers can be arranged in an array so as to provide thermal rectification on a macroscopic scale.

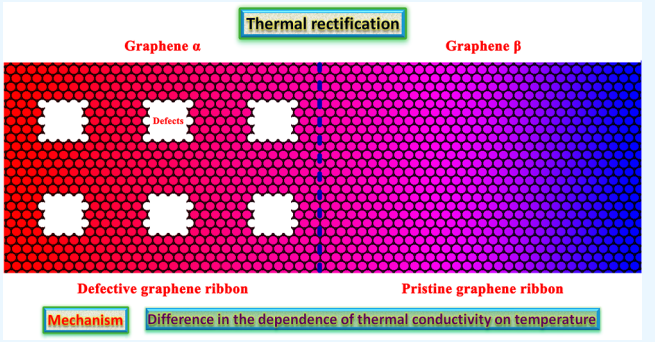

1. INTRODUCTION

Thermal rectification is a physical phenomenon in which the rate of heat transfer along a specific axis is controlled by the direction of temperature gradient.[1,2] Thermally rectifying technology provides the opportunity to manufacture novel thermal rectification device designs, which offer improvements in thermal management by controlling heat flux.[3,4] There are unique advantages associated with this type of heat-transfer device with the ability to rectify a heat flow[5,6] since thermal management has become essential to modern microelectronics. There are numerous configurations of thermally rectifying materials, and numerous studies on rectification mechanisms have been performed,[7,8] with primary interest focused on thermally rectifying properties and behaviors.[9,10] Unfortunately, the literature appears to be consistent in describing the phenomena of thermal rectification as complex and not well understood.[2] Undaunted by the complexity of this phenomena, there have been numerous attempts to improve the effectiveness and efficiency of thermal rectification.[11,12] Some limited successes have been claimed for certain types of thermally rectifying materials.

Thermal rectification can be achieved on the macro-scale and on a microscopic level, and there are different mechanisms accounting for thermal rectification, depending upon the nanostructured geometry, non-uniform mass distributions, material properties, and surface structures and characteristics. For many thermally rectifying materials, detailed mechanisms require development, such as the difference in the dependence of thermal conductivity on temperature,[13,14] thermal potential barriers at interfaces,[15,16] the effect of surface structures on

Received: April 2, 2022
Accepted: July 19, 2022
Published: August 1, 2022

© 2022 The Authors. Published by American Chemical Society

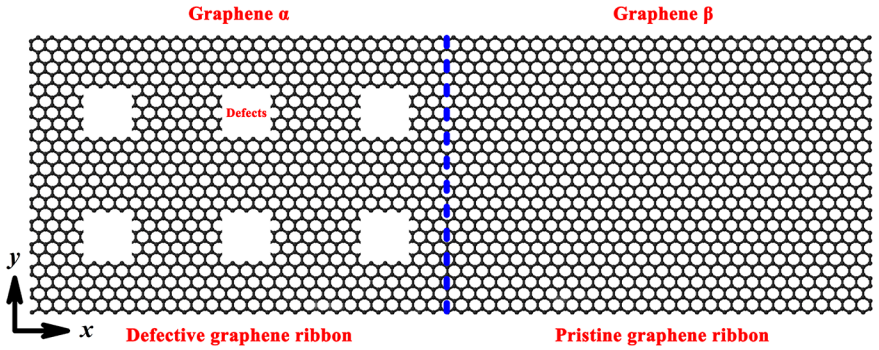

Figure 1. Schematic representation of the thermally rectifying material composed of pristine and defective graphene ribbons. The pristine graphene ribbons are defect-free. Thermal rectification appears through the introduction of vacancy defects. The thermal conductivity is heavily dependent on temperature. There is difference in temperature dependence between pristine and defective graphene ribbons. The thermal conductivity is affected by the nature and arrangements of the defects. How the thermal properties change with defects are investigated theoretically. The heat flow is defined in the *x*-direction, that is, in the length direction.

thermal conductivity at interfaces,[17,18] quantum thermal systems,[19,20] anharmonic lattices,[21,22] and nanostructured asymmetry.[23,24] The anharmonic lattices typically have a one-dimensional nanostructure.[25,26] Typical examples of nanostructured asymmetry are nanotubes with an axially non-uniform mass distribution,[27,28] nanostructured interfaces,[29,30] and the asymmetric geometrical shape of a nanostructure,[31,32] for example, asymmetric graphene sheets.[33,34] Thermal rectification has been demonstrated for nanostructures that are conductive, for example, carbon nanotubes, and for linear nanostructures that are electrical insulators, for example, boron nitride nanotubes.[27,28] These mechanisms can be used in the design or modification of thermally rectifying materials to optimize the methods for forming thermally rectifying nanostructures and to improve the levels of thermal rectification.

The rectification mechanisms provide engineers with tools to better understand and describe thermal rectification processes, which would have important implications for thermal management, thermal circuits, and the field of phononics in general. Linear nanostructures have very high intrinsic thermal conductance, but they normally display no thermal rectification effects. Correct rectification mechanisms are an important part of accurate predictive modeling. However, it is still a long-sought goal to achieve high levels of thermal rectification and to make accurate predictions using theoretical methods with the existing mechanisms.[35,36] In recent years, theoretical proposals for thermal rectifiers have been put forward, but these involve complex coupling between individual atoms and substrates, which are difficult to construct as actual devices.[37,38] Asymmetric thermal conduction has been achieved, but many theoretical methods are impractical for most applications. It would be highly desirable to have a simple, solid-state, asymmetric thermally rectifying material and to make predictions about the level of thermal rectification using a theoretical method.

The present study relates to a thermally rectifying material and, more particularly, to a graphene-based nanomaterial for controlling heat flux and the associated method determining the rectification coefficient. The nanomaterial has a rectification characteristic with respect to heat flow between two solid media of the same material for facilitating fabrication of a thermal rectification device. Restructured pristine and defective graphene ribbons were used as a thermally rectifying material to provide an optimum level of thermal rectification. Specially arranged vacancy defects were introduced into one end of the nanostructure to produce an axially non-uniform mass distribution. Nanofabrication methods have the potential for efficiently constructing such a thermal rectification design. Modified Monte Carlo methods were used to investigate the effects of defect size and shape, vacancy concentration, and ribbon length on the thermal rectification properties. Anharmonic lattice dynamics calculations were carried out in order to be able to obtain the frequency-dependent phonon properties. The effects on thermal conductivity and rectification coefficient were evaluated by a deviational Monte Carlo method. The objective of this study is to provide a nanoscale system that conducts heat asymmetrically with a maximum rectification coefficient. Particular emphasis is placed on the development of a method for designing and operating a thermally rectifying system, particularly a graphene-based nanostructure material with improved thermal rectification properties.

2. METHODS

2.1. Physical System. The present study relates to a thermal rectifier configured to rectify a heat flow. This thermal rectifier with the ability to rectify a heat flow includes a combination of two solid media with mutually different thermal conductivity characteristics. In order to improve the degree of freedom of design, desirably, the two media are of the same material, graphene. The thermally rectifying material composed of pristine and defective graphene ribbons is schematically illustrated in Figure 1. For the sake of convenience, the pristine and defective graphene ribbons are referred to as graphene α and β, respectively. Structural defects do not appear in the pristine graphene ribbons. Through the introduction of specially arranged vacancy defects, thermal rectification appears in the material. Thermal rectification is achieved due to the difference in temperature dependence of thermal conductivity.

The thermal conductivity of graphene exhibits significant temperature dependence. More specifically, the thermal conductivity is heavily dependent on temperature,[39,40] with temperature dependence based on a power function.[41,42] However, there is significant difference in temperature dependence between pristine and defective graphene ribbons so that the material has certain unique thermal properties. The difference arises because the thermal conductivity is also affected significantly by the nature and arrangements of the

https://doi.org/10.1021/acsomega.2c02041
ACS Omega 2022, 7, 28030−28040

defects. More specifically, defects can reduce the thermal conductivity of graphene by an order of magnitude or more.[43,44] Imperfections in the defective graphene ribbons changes not only the thermal properties of the crystal but also the dependence on temperature. Heat flux which flows from the defective graphene ribbon maintained at a high temperature to the pristine graphene ribbon maintained at a low temperature is greater in intensity than heat flux which flows from the pristine graphene ribbon maintained at a high temperature to the defective graphene ribbon maintained at a low temperature.[43,44] A thermal rectification characteristic can therefore be obtained. In the present study, how the thermal properties change with defects are investigated theoretically. The defects can be of any shape, and the size may vary. The number of defects may also vary as needed.

2.2. Traditional Monte Carlo Methods. The Boltzmann transport equation is given by

$$\frac{\partial f}{\partial t} + v_{\text{group}}\nabla f = -(f - f^{\text{loc}})(\tau(\omega, p, T))^{-1} \tag{1}$$

in which f is the phonon distribution function in the phase space of the system, t is the time, v_{group} is the group velocity, ω is the phonon radial frequency, p is the phonon polarization, f^{loc} is the local equilibrium distribution function, τ is the relaxation time, and T is the temperature. The pseudotemperature is the temperature of an equilibrium distribution of phonons with the same energy density as the actual energy density. The relaxation time approximation is introduced, which is a commonly used simplification.

The following approximation is assumed

$$\frac{1}{8\pi^3}f(t, \mathbf{x}, \mathbf{k}, p) \approx N_{\text{eff}}\sum_i \delta^3(\mathbf{x} - \mathbf{x}_i)\delta^3(\mathbf{k} - \mathbf{k}_i)\delta_{p,p_i} \tag{2}$$

wherein $\mathbf{x}$ is the spatial position vector, $\mathbf{k}$ is the phonon wave vector, N_{eff} is the total number of phonons in each phonon branch, and δ is a delta function. Particle i is denoted by the subscript i. This expression can be written in terms of polar coordinates and frequency as follows

$$\frac{1}{4\pi}D(\omega, p)f(t, \mathbf{x}, \omega, \theta, \varphi, p)\sin(\theta) \approx N_{\text{eff}}\sum_i \delta^3(\mathbf{x} - \mathbf{x}_i)\delta(\omega - \omega_i)\delta(\theta - \theta_i)\delta(\varphi - \varphi_i)\delta_{p,p_i} \tag{3}$$

where D is the density of states, θ is the polar angle, and φ is the azimuthal angle.

The density of states is expressed as a function of frequency and polarization

$$D(\omega, p) = \frac{1}{2\pi^2}k(\omega, p)^2(v_{\text{group}}(\omega, p))^{-1} \tag{4}$$

The Bose−Einstein statistics applies to the particles

$$N = V\int_0^{\omega_D}\sum_p D(\omega, p)f_T^{\text{eq}}(\omega)\mathrm{d}\omega \tag{5}$$

$$f_T^{\text{eq}} = (\exp(\hbar\omega(\mathbf{k}, p)(k_bT)^{-1}) - 1)^{-1} \tag{6}$$

in which V is the phase-space volume, ω_D is the Debye frequency, $\hbar$ is the reduced Planck constant, and k_b is the Boltzmann constant.

The local total energy is given by

$$E = N_{\text{eff}}\sum_i \hbar\omega_i = V\int_0^{\omega_D}\sum_p D(\omega, p)\hbar\omega(\mathbf{k}, p)(\exp(\hbar\omega(\mathbf{k}, p)(k_bT)^{-1}) - 1)^{-1}\mathrm{d}\omega \tag{7}$$

Accordingly, the local total pseudoenergy $\hat{E}$ is given by

$$\hat{E} = N_{\text{eff}}\sum_i \hbar\omega_i\tau(\omega_i, p_i, T)^{-1} = V\int_0^{\omega_D}\sum_p D(\omega, p)\hbar\omega(\mathbf{k}, p)\tau(\omega, p, T)^{-1}(\exp(\hbar\omega(\mathbf{k}, p)(k_bT)^{-1}) - 1)^{-1}\mathrm{d}\omega \tag{8}$$

The probability of phonon scattering P_i is given by

$$P_i = 1 - \exp(-\Delta t(\tau(\omega_i, p_i, T))^{-1}) \tag{9}$$

2.3. Energy-Based Formulation. Accuracy can be improved by introducing an energy-based formulation.[45,46] This formulation is effective in conserving energy in the relaxation time approximation.[47,48] The energy-based Boltzmann transport equation is given by

$$\frac{\partial e}{\partial t} + v_{\text{group}}\nabla e = -(e - e^{\text{loc}})(\tau(\omega, p, T))^{-1} \tag{10}$$

$$e = \hbar\omega f \tag{11}$$

$$e^{\text{loc}} = \hbar\omega f^{\text{loc}} \tag{12}$$

wherein e is the energy distribution function in the phase space of the system, ∇ is the gradient operator, and e^{loc} is the local energy equilibrium distribution function.

The energy-based phonon distribution function can be written as

$$e \approx 8\pi^3\varepsilon_{\text{eff}}\sum_i \delta^3(\mathbf{x} - \mathbf{x}_i)\delta^3(\mathbf{k} - \mathbf{k}_i)\delta_{p,p_i} \tag{13}$$

$$\varepsilon_{\text{eff}} = N_{\text{eff}}\hbar\omega \tag{14}$$

in which ε_{eff} is the effective energy carried by each particle.

2.4. Deviational Formulation. Modifications to the energy-based formulation are made to significantly reduce the statistical uncertainty for solving the Boltzmann transport equation. The method of control variates is introduced to solve the problem.[49,50] The moments of a specific phonon distribution function can be written as

$$\int Rf\,\mathrm{d}\mathbf{x}\mathrm{d}\mathbf{c} = \int R(f - f^{\text{eq}})\mathrm{d}\mathbf{x}\mathrm{d}\mathbf{c} + \int Rf^{\text{eq}}\,\mathrm{d}\mathbf{x}\mathrm{d}\mathbf{c} \tag{15}$$

where R is the moment and $\mathbf{c}$ is the molecular velocity vector.

The energy equilibrium distribution function can be written as

$$e_{T_{\text{eq}}}^{\text{eq}}(\omega) = \hbar\omega(\exp(\hbar\omega(\mathbf{k}, p)(k_bT_{\text{eq}})^{-1}) - 1)^{-1} \tag{16}$$

in which T_{eq} is the equilibrium temperature.

The deviational formulation of the energy equilibrium distribution e^{d} is given by

$$\frac{\partial e^{\text{d}}}{\partial t} + v_{\text{group}}\nabla e^{\text{d}} = ((e^{\text{loc}} - e_{T_{\text{eq}}}^{\text{eq}}) - e^{\text{d}})(\tau(\omega, p, T))^{-1} \tag{17}$$

https://doi.org/10.1021/acsomega.2c02041
ACS Omega 2022, 7, 28030−28040

$$e^{\mathrm{d}} = e - e^{\mathrm{eq}}_{T_{\mathrm{eq}}} \tag{18}$$

This deviational energy distribution function can be written as

$$e \approx 8\pi^3 \varepsilon^d_{\mathrm{eff}} \sum_i s(i)\delta^3(\mathbf{x} - \mathbf{x}_i)\delta^3(\mathbf{k} - \mathbf{k}_i)\delta_{p,p_i} \tag{19}$$

$$s(i) = \pm 1 \tag{20}$$

in which $\varepsilon^d_{\mathrm{eff}}$ is the effective deviational energy carried by each particle and $s(i)$ is the sign of particle i. Deviational particles are defined, and the sign may be negative.

2.5. Deviational Algorithms. The deviational energy of the system can be estimated as follows

$$\Delta E = \int_0^{\omega_{\mathrm{D}}} \sum_p D(\omega, p)\hbar\omega((\exp(\hbar\omega(k_{\mathrm{b}}T)^{-1}) - 1)^{-1} - (\exp(\hbar\omega(k_{\mathrm{b}}T_{\mathrm{eq}})^{-1}) - 1)^{-1})\mathrm{d}\omega \tag{21}$$

Accordingly, the effective deviational energy can be determined based upon the number of particles.

The frequencies and polarizations can be estimated as follows

$$D(\omega, p)e^{\mathrm{d}}(\omega) = \hbar\omega D(\omega, p)(f^0 - (\exp(\hbar\omega(k_{\mathrm{b}}T_{\mathrm{eq}})^{-1}) - 1)^{-1}) \tag{22}$$

wherein f^0 is the initial phonon distribution function. Typically, the system is in equilibrium in the initial state. Accordingly, the above expression can be written as follows

$$D(\omega, p)e^{\mathrm{d}}(\omega) = \hbar\omega D(\omega, p)((\exp(\hbar\omega(k_{\mathrm{b}}T)^{-1}) - 1)^{-1} - (\exp(\hbar\omega(k_{\mathrm{b}}T_{\mathrm{eq}})^{-1}) - 1)^{-1}) \tag{23}$$

At temperatures above the equilibrium temperature, the deviational particles have a positive sign. At temperatures below the equilibrium temperature, the deviational particles have a negative sign.

In the scattering process, the deviational formulation is given by

$$\frac{\partial e^{\mathrm{d}}}{\partial t} = ((e^{\mathrm{loc}} - e^{\mathrm{eq}}_{T_{\mathrm{eq}}}) - e^{\mathrm{d}})(\tau(\omega, p, T_j))^{-1} \tag{24}$$

$$e^{\mathrm{loc}} - e^{\mathrm{eq}}_{T_{\mathrm{eq}}} = \hbar\omega((\exp(\hbar\omega(k_{\mathrm{b}}(T_{\mathrm{loc}})_j)^{-1}) - 1)^{-1} - (\exp(\hbar\omega(k_{\mathrm{b}}T_{\mathrm{eq}})^{-1}) - 1)^{-1}) \tag{25}$$

where T_j is the temperature in the cell j and $(T_{\mathrm{loc}})_j$ is the local pseudotemperature in cell j.

The probability of phonon scattering in cell j is given by

$$P(\omega_i, p_i, T_j) = 1 - \exp(-\Delta t(\tau(\omega_i, p_i, T_j))^{-1}) \tag{26}$$

The deviational energy in cell j is given by

$$\Delta E_j = \varepsilon^d_{\mathrm{eff}}(N_j^+ - N_j^-) \tag{27}$$

in which N_j^+ is the number of positive particles in cell j and N_j^- is the number of negative particles in cell j.

The frequencies and polarizations can be estimated as follows

$$D(\omega, p)(e^{\mathrm{loc}} - e^{\mathrm{eq}}_{T_{\mathrm{eq}}})(\tau(\omega, p, T_j))^{-1} = \hbar\omega D(\omega, p)(\tau(\omega, p, T_j))^{-1} \cdot((\exp(\hbar\omega(k_{\mathrm{b}}(T_{\mathrm{loc}})_j)^{-1}) - 1)^{-1} - (\exp(\hbar\omega(k_{\mathrm{b}}T_{eq})^{-1}) - 1)^{-1}) \tag{28}$$

2.6. Anharmonic Lattice Dynamics Calculations. An important step in performing Monte Carlo simulations is to define the phonon properties. The phonon properties are temperature-dependent. Anharmonic lattice dynamics has a wide range of applications,[51,52] for example, understanding the characteristics of thermal transport at the nanoscale.[53,54] Anharmonic lattice dynamics calculations are carried out, and the interatomic force constants are calculated using density functional perturbation theory. The Monkhorst−Pack k-points are used with a 32 × 32 grid to define the accuracy of the Brillouin zone sampling. An energy cutoff is used to fix the number of planewaves in the basis set. An energy cutoff value of 750 eV is specified. The charge density is determined by an energy cutoff value of 6000 eV. The ultrasoft pseudopotential scheme is employed. A local exchange−correlation functional is implemented by applying the local density approximation. A lattice constant of 0.246 nm is considered. The length of the covalent bonds is 0.142 nm.

A structural defect is represented as a blocked region of a given size and shape. On reaching the boundary of a structural defect, the direction of phonon propagation is re-assigned using the two-dimensional diffuse reflection model[55,56] following Lambert's cosine law. It is realized by generating a random number $R' \in (-1, 1)$ and by setting $\theta' = \arcsin R'$, in which θ' is the angle of incidence with respect to the normal of the boundary. Randomization is performed using the same method for the boundaries wherein the phonons are emitted. The accuracy of the method depends upon a variety of factors, including the size and shape of each defect and the arrangement of the defects.

To eliminate the effect arising from phonon-edge scattering, periodic boundary conditions are applied to the graphene-based nanostructure. More specifically, periodic boundary conditions are used in a direction perpendicular to the direction of heat flow. Periodic boundary conditions are also used in the direction of heat flow to determine the thermal conductivity of graphene. Temperature boundary conditions are used to determine the thermal conductivity of graphene ribbons by specifying the temperature at each boundary.

The temperature difference between the boundaries is maintained at a constant level, 0.02 K. To determine the thermal conductivity, the temperature at the boundaries is specified as T_{eq} + 0.01 K and T_{eq} − 0.01 K.

2.7. Thermal Conductivity Calculations. The relaxation time is temperature-dependent, with temperature dependence based on a power function. The relaxation time is given by

$$\tau(T) = \tau_0\left(\frac{T}{T_0}\right)^n \tag{29}$$

$$T_0 = 0.5(T_\alpha + T_\beta) \tag{30}$$

wherein τ_0 is the relaxation time for a specific vibrational mode and phonon frequency, T_0 is the mean temperature, n is the power-law exponent, T_α is the temperature of graphene α, and T_β is the temperature of graphene β.

The temperature index can be estimated as follows

https://doi.org/10.1021/acsomega.2c02041
ACS Omega 2022, 7, 28030−28040

$$\lambda(T) = \lambda_{i,0}\left(\frac{T}{T_0}\right)^n \tag{31}$$

in which λ is the thermal conductivity and λ_0 is the thermal conductivity for a specific vibrational mode and phonon frequency.

The effective thermal conductivity λ_{eff} can be estimated by using the law of heat conduction

$$\lambda_{eff} = -\left(\frac{q}{l_y l_z}\right)\cdot\left(\frac{\Delta T}{l_x}\right)^{-1} \tag{32}$$

in which q is the amount of heat transferred per unit time; l is the length; and x, y, and z are the Cartesian coordinates.

2.8. Thermal Rectification Calculations. The rectification coefficient ε is defined as follows[57,58]

$$\varepsilon = (q^+ - q^-)\cdot(q^-)^{-1} \tag{33}$$

in which the superscripts + and − denote the forward direction and the reverse direction, respectively. A direction in which heat flux of high intensity flows is defined as the forward direction, and a direction in which heat flux of low intensity flows is defined as the reverse direction. The heat flux flowing in the reverse direction is smaller, in terms of intensity, than the heat flux flowing in the forward direction.

The absolute thermal resistance at the mean temperature R_0 is defined as follows[59,60]

$$R_0 = l_x\cdot(\lambda_0 l_y l_z)^{-1} \tag{34}$$

where λ_0 is the thermal conductivity at the mean temperature. The absolute thermal resistance is the reciprocal of thermal conductance. The thermal resistance ratio ρ is defined as follows

$$\rho = \frac{R_{0,\alpha}}{R_{0,\beta}} \tag{35}$$

wherein the subscripts α and β denote the graphene index.

The dimensionless heat flux q' is defined as

$$q' = q(R_{0,\alpha} + R_{0,\beta})\cdot(T_0)^{-1} \tag{36}$$

The dimensionless temperature θ is defined as

$$\theta = \frac{T}{T_0} \tag{37}$$

The dimensionless temperature difference Δ is defined as

$$\Delta = (T_\alpha - T_\beta)\cdot(T_0)^{-1} \tag{38}$$

$$\theta_\alpha = 1 + \frac{\Delta}{2} \tag{39}$$

$$\theta_\beta = 1 - \frac{\Delta}{2} \tag{40}$$

A particular solution is that the power-law exponent is 0. In this case, the thermal conductivity does not depend on temperature or stays approximately constant. For zero-order solutions, the dimensionless temperature and heat flux are given by

$$\theta' = 1 + \frac{\Delta}{2}(\rho - 1)(\rho + 1)^{-1} \tag{41}$$

$$q' = \Delta \tag{42}$$

in which θ' is the dimensionless interfacial temperature.

When small perturbations are imposed on the system, the dimensionless interfacial temperature can be written as

$$\theta' = 1 + d + \frac{\Delta}{2}(\rho - 1)(\rho + 1)^{-1} \tag{43}$$

$$d = \theta' - \theta_0' \tag{44}$$

in which θ_0' is the dimensionless interfacial temperature when the thermal conductivity does not depend on temperature.

Under small perturbation conditions, the dimensionless temperature is very close to unity. In such a context, the dimensionless temperature is expanded as a Taylor series in the dimensionless temperature difference. A second-order Taylor series expansion of the dimensionless temperature of graphene α can be written compactly as follows[59,60]

$$\theta_\alpha = 1 + \frac{1}{2}(n+1)\Delta + \frac{1}{8}n(n+1)\Delta^2 \tag{45}$$

The dimensionless heat flux is given by

$$q' = \Delta + \frac{1}{2}(n_\alpha - n_\beta)(\rho^{1/2} + \rho^{-1/2})^{-2}\Delta^2 \tag{46}$$

The rectification coefficient can be written as follows

$$\varepsilon = (q'(\Delta) + q'(-\Delta))\cdot(-q'(-\Delta))^{-1} \tag{47}$$

The dimensionless heat flux can be integrated into the rectification coefficient, yielding

$$\varepsilon = ((n_\alpha - n_\beta)\Delta(\rho^{1/2} + \rho^{-1/2})^{-2})\cdot\left(1 - \frac{1}{2}(n_\alpha - n_\beta)\Delta(\rho^{1/2} + \rho^{-1/2})^{-2}\right)^{-1} \tag{48}$$

The rectification coefficient can be approximated as follows

$$\varepsilon = (n_\alpha - n_\beta)\Delta(\rho^{1/2} + \rho^{-1/2})^{-2} \tag{49}$$

The thermally rectifying material composed of graphene ribbons is schematically illustrated.

3. RESULTS AND DISCUSSION

3.1. Thermal Conductivity. The effect of length on the thermal conductivity of pristine graphene ribbons is illustrated in Figure 2. The pristine graphene ribbons vary considerably in length. The length is 200, 500, 1000, and 10,000 nm. The temperature varies from 200 to 600 K. The calculated results of the power-law exponent are also presented in Figure 2. Longer graphene nanoribbons exhibit an excellent heat conduction property. However, the thermal conductivity decreases with the decrease of the length due to phonon-boundary scattering. Phonon-boundary scattering positively affects the dependence of thermal conductivity on temperature. The power-law exponent is 0.27, −0.36, −0.77, and −0.98. As the length decreases, a change of the power-law exponent is made from negative to positive. In this case, phonon-boundary scattering becomes dominant, while the effect of anharmonic phonon−phonon scattering becomes insignificant.

The effect of defects on the thermal conductivity of defective graphene ribbons is illustrated in Figure 3. The length of the graphene ribbons is 200 nm, and vacancies occur in the crystalline material. The crystallographic defects are approximately square in shape with a side length of about 1.0 nm. The

https://doi.org/10.1021/acsomega.2c02041
ACS Omega 2022, 7, 28030−28040

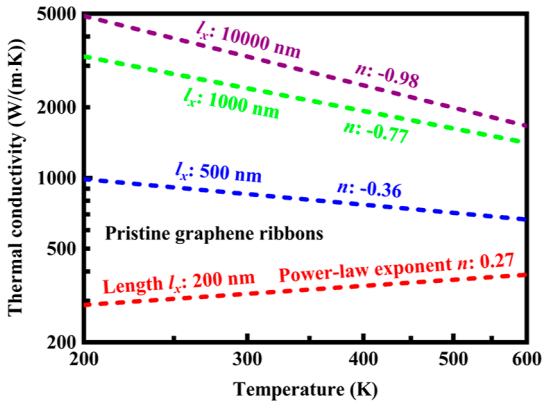

Figure 2. Effect of length on the thermal conductivity of pristine graphene ribbons. The calculated results of the power-law exponent are also presented.

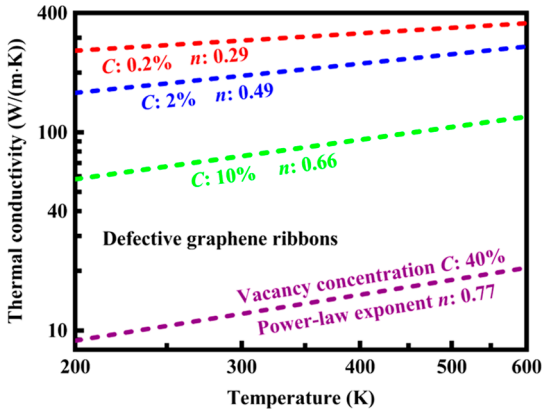

Figure 3. Effect of defects on the thermal conductivity of defective graphene ribbons. The length of the graphene ribbons is 200 nm, and vacancies occur in the crystalline material.

vacancy concentration C is 0.2, 2, 10, and 40%. The temperature varies from 200 to 600 K. The vacancy defects greatly affect the thermal properties of graphene ribbons. Defective graphene ribbons vary significantly in thermal conductivity with the vacancy concentration. More specifically, the graphene ribbons with the lowest number of defects typically have high thermal conductivity. The thermal conductivity at higher vacancy concentrations becomes sufficiently low as compared with that at lower vacancy concentrations, as shown in Figure 3. The thermal conductivity decreases with the increase of the vacancy concentration due to phonon scattering from defects. The thermal conductivity at higher vacancy concentrations is limited by the scattering of phonons at lattice defects.[61,62] The effect of temperature on thermal conductivity is different for the pristine and defective graphene ribbons, as shown in Figures 2 and 3. Defect scattering positively affects the dependence of thermal conductivity on temperature. The power-law exponent of temperature dependence is 0.29, 0.49, 0.66, and 0.77. The power-law exponent increases with the increase of the vacancy concentration. This implies that the dominant scattering mechanism is defect scattering under the physical conditions of interest.

The defects significantly affect the properties of phonon transport, making it possible to modulate the temperature dependence of thermal conductivity. By nanostructuring graphene ribbons with structural defects, it is possible to effectively increase the Debye temperature, which will eventually lead to positive temperature dependence. It has been demonstrated that the utilization of nanostructuring methods can modulate the temperature dependence of thermal conductivity.[63,64] As the length of the graphene ribbons decreases and the vacancy concentration increases, the effects of boundary and defect scatterings become more remarkable, which will eventually lead to a decrease in thermal conductivity. Additionally, these extrinsic scatterings largely modulate the temperature dependence of thermal conductivity, which will eventually lead to an increase in the power-law exponent of temperature dependence, thereby making it possible to change the power-law exponent from negative to positive. This phenomenon arises due to the diminished role of intrinsic temperature dependence since the phonon−phonon scattering becomes less dominant than the phonon-boundary and phonon-defect scattering. For example, when graphene ribbons are short, the thermal conductivity may increase with temperature, which is consistent with the results available in the literature.[65,66] The precise critical length value varies depending upon a variety of factors.

Thermal rectification is achieved since the thermal conductivity varies differently with respect to temperature between the pristine and defective graphene ribbons, as shown in Figures 2 and 3. The rectification coefficient increases with a decrease in the length of defective graphene ribbons or an increase in the vacancy concentration, the length of pristine graphene ribbons, or the magnitude of the difference between the power-law exponents, as defined by eq 49 and illustrated in Figures 2 and 3. However, an impedance mismatch problem exists since the thermal resistance ratio does deviate too far from unity. Variations in defect shape and dimensions can be used to optimize tradeoffs between competing factors such as the thermal resistance ratio and the difference between the power-law exponents. The effects of defect shape and dimensions are investigated in order to understand what factors influence thermally rectifying behavior.

The effect of defect size on the thermal conductivity of graphene ribbons is illustrated in Figure 4. The length of the graphene ribbons is 200 nm, and the defect size is about 1.0, 2.0, 3.0, and 4.0 nm. The size of defects varies while maintaining the vacancy concentration constant. The calculated results of the power-law exponent are also presented in Figure 4. The defect size considerably affects the thermal

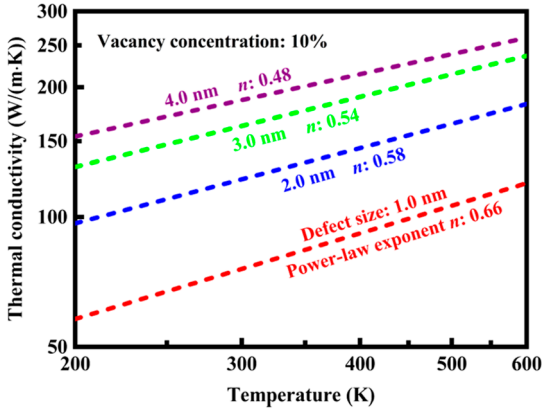

Figure 4. Effect of defect size on the thermal conductivity of defective graphene ribbons. The length of the graphene ribbons is 200 nm.

https://doi.org/10.1021/acsomega.2c02041
ACS Omega 2022, 7, 28030−28040

properties of graphene ribbons. The thermal conductivity increases with the increase of the defect size. As the defect size increases, the number of defects decreases, associated with a decrease in the total length of the edges of the defects in the crystal structure. The increase of defect size will lead to a decrease in the strength of defect scattering and therefore an increase in the thermal conductivity, as shown in Figure 4. Accordingly, the power-law exponent decreases with the increase of the defect size. As the size of crystallographic defects is increased to a certain extent, the power-law exponent is expected to be close to that of pristine graphene ribbons.

The effect of defect shape on the thermal conductivity of defective graphene ribbons is illustrated in Figure 5. Two shape

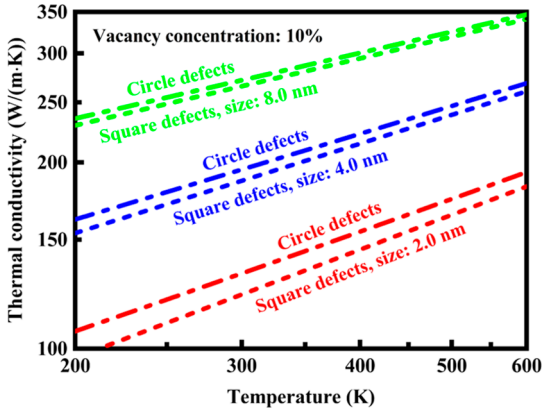

Figure 5. Effect of defect shape on the thermal conductivity of defective graphene ribbons. The length of the graphene ribbons is 200 nm.

cases are considered here: square and circle. The defect shape varies while maintaining a constant vacancy concentration. The vacancy concentration is 10%, and the length of the graphene ribbons is 200 nm. There is little difference in the total length of the edges of the crystallographic defects between the two shape cases considered. As a result, the thermal conductivity varies insignificantly between different crystallographic defect shapes, as shown in Figure 5. As the defect size increases, the difference in thermal conductivity between different defect shapes becomes smaller, especially at higher temperatures. In particular, the difference is very small when the defect size is about 8.0 nm. Therefore, the defect shape has only a small effect on the thermal conductivity, which is different from the effect of defect size. This means that the thermal conductivity does not depend heavily upon the shape of defects for the nanostructure used. In such a context, only square defects are considered in the present study.

3.2. Thermal Rectification. The effect of the length of pristine graphene ribbons on the rectification coefficient is illustrated in Figure 6. The length of defective graphene ribbons is 200 nm. The defect size is about 1.0 nm, and the vacancy concentration is 5, 10, 15, and 20%. The length of pristine graphene ribbons plays an important role in the rectification coefficient. As the length of pristine graphene ribbons increases, the rectification coefficient first increases and then decreases. Therefore, longer pristine graphene ribbons do not necessarily lead to higher levels of thermal rectification. Additionally, the rectification coefficient depends upon the vacancy concentration. Higher vacancy concentrations will lead to a maximum available rectification coefficient, thereby

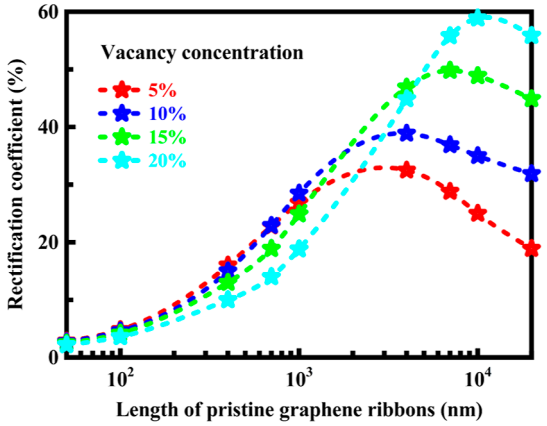

Figure 6. Effect of the length of pristine graphene ribbons on the rectification coefficient. The defect size is about 1.0 nm, and the length of defective graphene ribbons is 200 nm.

increasing forward heat flux and reducing reverse heat flux. The maximum rectification coefficient is approximately 60%. The maximum available rectification coefficient decreases with the decrease of the vacancy concentration.

The effect of the length of defective graphene ribbons on the rectification coefficient is illustrated in Figure 7. The length of

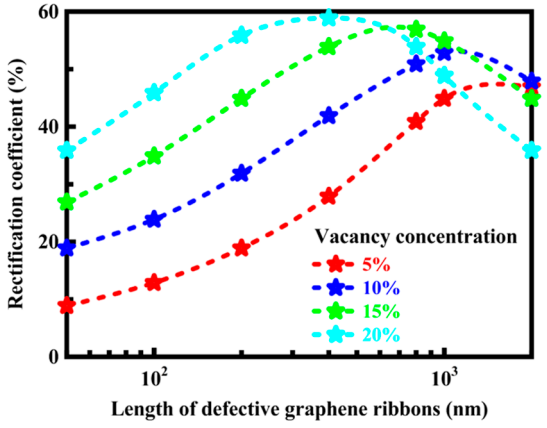

Figure 7. Effect of the length of defective graphene ribbons on the rectification coefficient. The defect size is about 1.0 nm, and the length of pristine graphene ribbons is 20 μm.

pristine graphene ribbons is 20 μm. The defect size is about 1.0 nm, and the vacancy concentration is 5, 10, 15, and 20%. The length of defective graphene ribbons strongly affects the rectification coefficient. As the length of defective graphene ribbons increases, the rectification coefficient first increases and then decreases, in a manner similar to the phenomenon of the effect of the length of pristine graphene ribbons, as shown in Figure 6. Longer defective graphene ribbons do not necessarily lead to higher levels of thermal rectification. Additionally, the vacancy concentration plays a vital role in the rectification coefficient, as discussed above. Higher vacancy concentrations are necessary to achieve the maximum rectification coefficient. In contrast, longer defective graphene ribbons are not essential for higher levels of thermal rectification.

A balance between competing factors can be used to determine the effect of the length of graphene ribbons. The two competing factors are the power-law exponents and the thermal resistance ratio, as discussed above. The competing

https://doi.org/10.1021/acsomega.2c02041
ACS Omega 2022, 7, 28030−28040

factors can be balanced to determine the appropriate length of graphene ribbons for thermal rectification. Therefore, the effects of the length of graphene ribbons on the two competing factors are investigated, and the results are presented below.

The effect of the length of pristine graphene ribbons on the difference in power-law exponent is illustrated in Figure 8. As

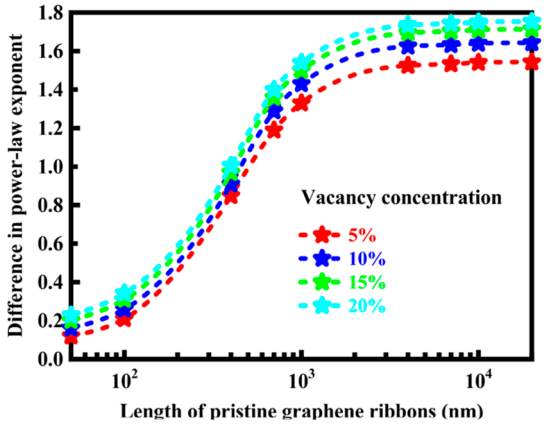

Figure 8. Effect of the length of pristine graphene ribbons on the difference in power-law exponent. The defect size is about 1.0 nm, and the length of defective graphene ribbons is 200 nm.

the vacancy concentration or the length of pristine graphene ribbons increases, the difference in power-law exponent increases. The length of pristine graphene ribbons significantly affects the difference in power-law exponent. In contrast, the vacancy concentration plays a relatively minor role in the difference in power-law exponent, regardless of the length of pristine graphene ribbons. The effect of the length of defective graphene ribbons on the difference in power-law exponent is illustrated in Figure 9. The difference in power-law exponent

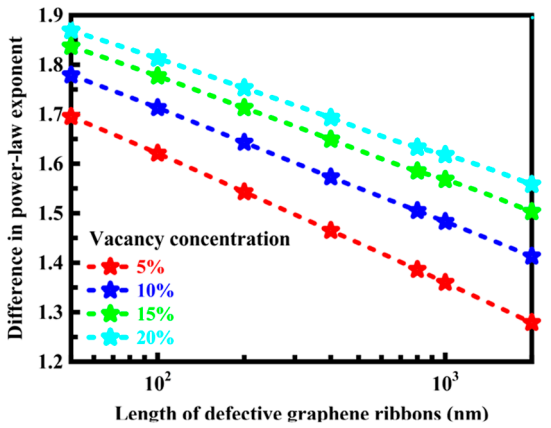

Figure 9. Effect of the length of defective graphene ribbons on the difference in power-law exponent. The defect size is about 1.0 nm, and the length of pristine graphene ribbons is 20 μm.

varies considerably, depending upon the vacancy concentration and the length of defective graphene ribbons. More specifically, the difference in power-law exponent increases with the increase of the vacancy concentration, but it decreases with the increase of the length of defective graphene ribbons, which is exactly the opposite of the effect of the length of pristine graphene ribbons. The rectification coefficient is proportional to the difference in power-law exponent, as expressed by eq 49. Therefore, longer pristine graphene ribbons and shorter defective graphene ribbons may be used to take advantage of their large differences in power-law exponent, which allows for a higher rectification coefficient.

The effects of the length of pristine and defective graphene ribbons on the thermal resistance ratio are illustrated in Figures 10 and 11, respectively. The thermal resistance ratio depends

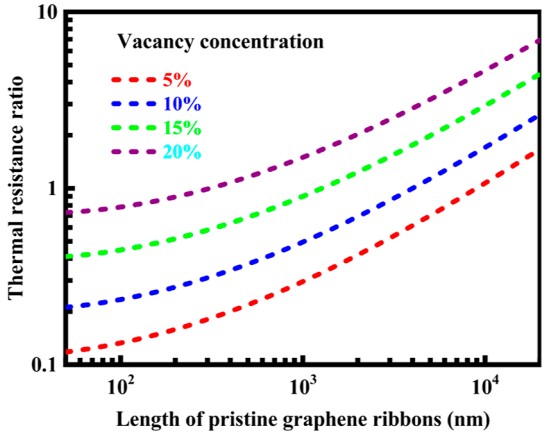

Figure 10. Effect of the length of pristine graphene ribbons on the thermal resistance ratio. The defect size is about 1.0 nm, and the length of defective graphene ribbons is 200 nm.

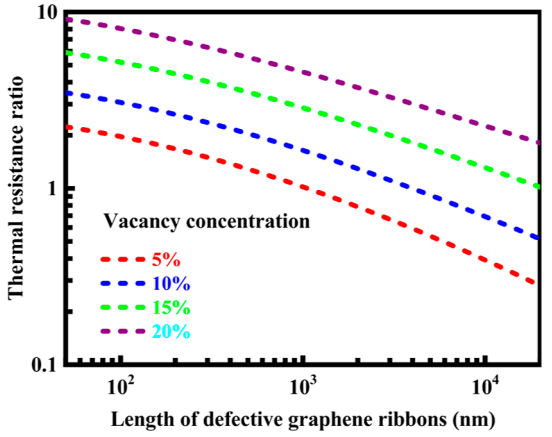

Figure 11. Effect of the length of defective graphene ribbons on the thermal resistance ratio. The defect size is about 1.0 nm, and the length of pristine graphene ribbons is 20 μm.

strongly upon the relative length of pristine and defective graphene ribbons. More specifically, the thermal resistance ratio increases with the increase of the length of pristine graphene ribbons and with the decrease of the length of defective graphene ribbons. However, an impedance mismatch problem exists when the thermal resistance ratio deviates too far from unity. The rectification coefficient depends heavily upon the thermal resistance ratio, as expressed by eq 49. When the thermal resistance ratio is close to unity, the maximum rectification coefficient can be achieved. When the thermal resistance ratio deviates from unity, the rectification coefficient decreases. Consequently, longer graphene ribbons do not necessarily lead to higher levels of thermal rectification. Suitable selection of the length of pristine and defective graphene ribbons is essential for thermal rectification.

https://doi.org/10.1021/acsomega.2c02041
ACS Omega 2022, 7, 28030−28040

The effect of defect size on the rectification coefficient is illustrated in Figure 12. The length of pristine graphene

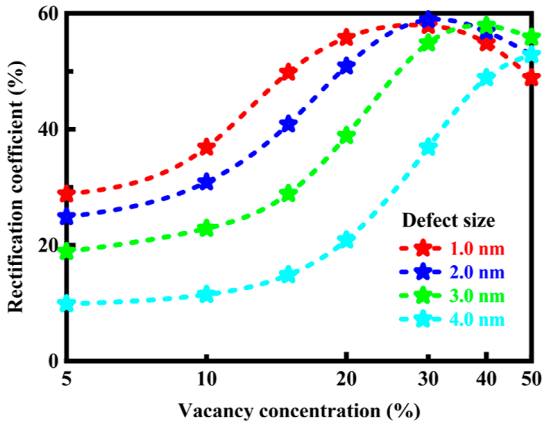

Figure 12. Effect of defect size on the rectification coefficient. The length of pristine graphene ribbons is 7 μm, and the length of defective graphene ribbons is 200 nm.

ribbons is 7 μm, and the length of defective graphene ribbons is 200 nm. The defect size is about 1.0, 2.0, 3.0, and 4.0 nm. When the defect size falls within a range of 1.0−4.0 nm, a maximum rectification coefficient of about 60% can be obtained for the range of vacancy concentrations between 30 and 50%. As the defect size increases, the vacancy concentration at which the maximum rectification coefficient is obtained increases. The rectification coefficient varies significantly with the defect size and the vacancy concentration. However, the difference in maximum rectification coefficient is small between the graphene ribbons with different defect sizes. As the vacancy concentration increases, the rectification coefficient first increases and then decreases.

The effect of defect size on the thermal conductivity of defective graphene ribbons is illustrated in Figure 13 when a maximum rectification coefficient is achieved. The defect size is about 1.0, 2.0, 3.0, and 4.0 nm. The vacancy concentration is determined by the maximum rectification coefficient, and the length of defective graphene ribbons is 200 nm. The defect size varies greatly, but the difference in thermal conductivity is not

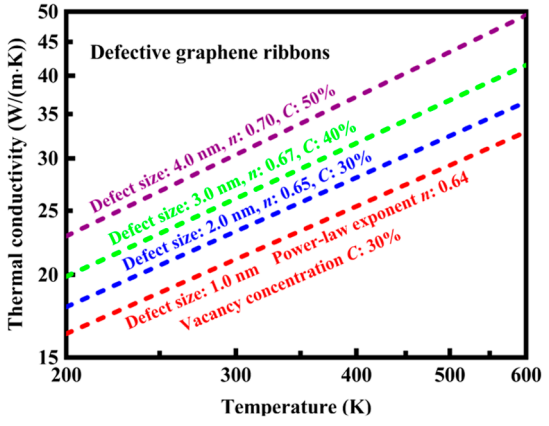

Figure 13. Effect of defect size on the thermal conductivity of defective graphene ribbons when a maximum rectification coefficient is achieved. The length of defective graphene ribbons is 200 nm. The vacancy concentration is determined by the maximum rectification coefficient.

significant. Accordingly, the maximum available rectification coefficient does not vary significantly with the defect size, as shown in Figure 12. Additionally, there is little difference in power-law exponent between the graphene ribbons with different defect sizes. The thermal conductivity increases with the increase of the defect size and decreases with the increase of the vacancy concentration, as discussed above. The thermal conductivity increases as the defect size increases from 1.0 to 4.0 nm and the vacancy concentration increases from 30 to 50%, as shown in Figure 13. Accordingly, there is a small increase in power-law exponent.

The effect of vacancy concentration on the rectification coefficient is illustrated in Figure 14. The length of defective

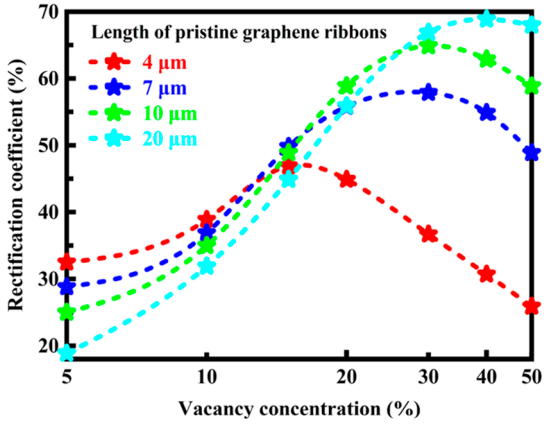

Figure 14. Effect of vacancy concentration on the rectification coefficient. The defect size is about 1.0 nm, and the length of defective graphene ribbons is 200 nm.

graphene ribbons is 200 nm, and the length of pristine graphene ribbons is 4, 7, 10, and 20 μm. The defect size is about 1.0 nm. As the vacancy concentration increases, the rectification coefficient first increases and then decreases, thereby changing the relative intensity of forward and reverse heat fluxes. For the longer graphene ribbons, a significant difference in rectification coefficient is identified between different vacancy concentrations. In contrast, for the shorter graphene ribbons, the difference in rectification coefficient is small between different vacancy concentrations. When the pristine graphene ribbons are 20 μm in length, a maximum rectification coefficient of about 70% can be obtained for the range of vacancy concentrations between 30 and 50%, as shown in Figure 14. However, the maximum rectification coefficient decreases with the decrease of the length of pristine graphene ribbons.

4. CONCLUSIONS

The present study was focused primarily on the design and operation of a thermally rectifying system, particularly a graphene-based nanostructure material with improved thermal rectification properties. The effects of defect size and shape, vacancy concentration, and ribbon length on the thermal rectification properties were investigated by using modified Monte Carlo methods in order to achieve maximum rectification coefficients. The frequency-dependent phonon properties were determined by performing anharmonic lattice dynamics calculations. The following major conclusions can be drawn from this study.

https://doi.org/10.1021/acsomega.2c02041
ACS Omega 2022, 7, 28030−28040

- A computational method has been developed, whereby the numerous variables used to determine the rectification coefficient can be summarized by two parameters: the power-law exponent and the thermal resistance ratio. The two defined variables provide a convenient method for design and operation of a rectification process in a thermal rectifier. Accordingly, the rectification coefficient can be obtained by solving a simple algebraic expression.
- The thermal conductance is asymmetric. The nanostructure exhibits asymmetric thermal conduction along its central axis, with a maximum available rectification coefficient of about 70%. The nanostructure has very high intrinsic thermal conductivity and displays thermal rectification effects. The thermal rectification effects can be attributed to the difference in the dependence of thermal conductivity on temperature.
- Graphene is an ideal material for thermal rectification. The nanoscale system allows heat to flow preferentially in one direction but retards the flow in the opposite direction. Vacancy defects can be introduced into one end of the nanostructure to produce an axially nonuniform mass distribution. The nanostructure conducts heat along its central axis differently in each direction.
- There are several structure factors that cause noticeable effects on the thermal rectification properties, including defect size, vacancy concentration, and ribbon length. However, the maximum available rectification coefficient does not vary significantly with the defect size. Additionally, the thermal rectification effects do not depend heavily upon the defect shape.
- Graphene-based nanostructure thermal rectifiers can be arranged in an array. The nanostructures are arranged approximately parallel. Such arrays can be made using any number of nanostructures so as to provide thermal rectification on a macroscopic scale.

AUTHOR INFORMATION

Corresponding Author

Junjie Chen − *Department of Energy and Power Engineering, School of Mechanical and Power Engineering, Henan Polytechnic University, Jiaozuo, Henan 454000, P.R. China;* orcid.org/0000-0001-8348-4896; Email: cjjmmm@163.com

Author

Lingyu Meng − *Department of Energy and Power Engineering, School of Mechanical and Power Engineering, Henan Polytechnic University, Jiaozuo, Henan 454000, P.R. China*

Complete contact information is available at: https://pubs.acs.org/10.1021/acsomega.2c02041

Notes

The authors declare no competing financial interest.

ACKNOWLEDGMENTS

This work was supported by the National Natural Science Foundation of China (no. 51506048).

REFERENCES

(1) Starr, C. The copper oxide rectifier. *J. Appl. Phys.* **1936**, *7*, 15−19.

(2) Roberts, N. A.; Walker, D. G. A review of thermal rectification observations and models in solid materials. *Int. J. Therm. Sci.* **2011**, *50*, 648−662.

(3) Terraneo, M.; Peyrard, M.; Casati, G. Controlling the energy flow in nonlinear lattices: A model for a thermal rectifier. *Phys. Rev. Lett.* **2002**, *88*, 094302.

(4) Chang, C. W.; Okawa, D.; Majumdar, A.; Zettl, A. Solid-state thermal rectifier. *Science* **2006**, *314*, 1121−1124.

(5) Casati, G. The heat is on - and off. *Nat. Nanotechnol.* **2007**, *2*, 23−24.

(6) Casati, G. Controlling the heat flow: Now it is possible. *Chaos* **2005**, *15*, 015120.

(7) Walker, D. G. Thermal rectification mechanisms including noncontinuum effects. *In 18th National & 7th ISHMT-ASME Heat and Mass Transfer Conference*; IIT Guwahati: India, 2006.

(8) Somers, R. R., II; Fletcher, L. S.; Flack, R. D. Explanation of thermal rectification. *AIAA J.* **1987**, *25*, 620−621.

(9) Latella, I.; Ben-Abdallah, P.; Nikbakht, M. Radiative thermal rectification in many-body systems. *Phys. Rev. B* **2021**, *104*, 045410.

(10) Kobayashi, W. Thermal-rectification coefficients in solid-state thermal rectifiers. *Phys. Rev. E* **2020**, *102*, 032142.

(11) Hu, S.; An, M.; Yang, N.; Li, B. A Series circuit of thermal rectifiers: An effective way to enhance rectification ratio. *Small* **2017**, *13*, 1602726.

(12) Li, N.; Ren, J.; Wang, L.; Zhang, G.; Hänggi, P.; Li, B. Colloquium: Phononics: Manipulating heat flow with electronic analogs and beyond. *Rev. Mod. Phys.* **2012**, *84*, 1045−1066.

(13) Marucha, C.; Mucha, J.; Rafałowicz, J. Heat flow rectification in inhomogeneous GaAs. *Phys. Status Solidi A* **1975**, *31*, 269−273.

(14) Marucha, C.; Mucha, J.; Rafałowicz, J. Phenomenological interpretation of heat flux volume rectification in Non-homogeneous media. *Phys. Status Solidi A* **1976**, *37*, K5−K7.

(15) Rogers, G. F. C. Heat transfer at the interface of dissimilar metals. *Int. J. Heat Mass Transfer* **1961**, *2*, 150−154.

(16) Moon, J. S.; Keeler, R. N. A theoretical consideration of directional effects in heat flow at the interface of dissimilar metals. *Int. J. Heat Mass Transfer* **1962**, *5*, 967−971.

(17) Powell, R. W.; Tye, R. P.; Jolliffe, B. W. Heat transfer at the interface of dissimilar materials: Evidence of thermal-comparator experiments. *Int. J. Heat Mass Transfer* **1962**, *5*, 897−902.

(18) Clausing, A. M. Heat transfer at the interface of dissimilar metals-the influence of thermal strain. *Int. J. Heat Mass Transfer* **1966**, *9*, 791−801.

(19) Wu, L.-A.; Segal, D. Sufficient conditions for thermal rectification in hybrid quantum structures. *Phys. Rev. Lett.* **2009**, *102*, 095503.

(20) Ojanen, T. Selection-rule blockade and rectification in quantum heat transport. *Phys. Rev. B: Condens. Matter Mater. Phys.* **2009**, *80*, No. 180301(R).

(21) Terraneo, M.; Peyrard, M.; Casati, G. Controlling the energy flow in nonlinear lattices: A model for a thermal rectifier. *Phys. Rev. Lett.* **2002**, *88*, 094302.

(22) Li, B.; Wang, L.; Casati, G. Thermal diode: Rectification of heat flux. *Phys. Rev. Lett.* **2004**, *93*, 184301.

(23) Otey, C. R.; Lau, W. T.; Fan, S. Thermal Rectification through Vacuum. *Phys. Rev. Lett.* **2010**, *104*, 154301.

(24) Roberts, N.; Walker, D. Phonon transport in asymmetric sawtooth nanowires. *ASME-JSME 2011 8th Thermal Engineering Joint Conference*; ASME-JSME: Honolulu, Hawaii, United States, 2011.

(25) Hu, B.; Yang, L.; Zhang, Y. Asymmetric heat conduction in nonlinear lattices. *Phys. Rev. Lett.* **2006**, *97*, 124302.

(26) Terraneo, M.; Peyrard, M.; Casati, G. Controlling the energy flow in nonlinear lattices: A model for a thermal rectifier. *Phys. Rev. Lett.* **2002**, *88*, 094302.

(27) Budaev, B. V.; Bogy, D. B. Thermal rectification in inhomogeneous nanotubes. *Appl. Phys. Lett.* **2016**, *109*, 231905.

(28) Chen, W.-J.; Feng, B.; Shao, C.; Yang, J.; Fan, L.; Ong, W.-L.; Chang, I.-L. Asymmetrical carbon nanotubes exhibit opposing thermal

rectification behaviors under different heat baths. *Int. J. Heat Mass Transfer* **2022**, *184*, 122341.
(29) Roberts, N. A.; Walker, D. G. Computational study of thermal rectification from nanostructured interfaces. *J. Heat Transfer* **2011**, *133*, 092401.
(30) López-Suárez, M.; Royo, M.; Rurali, R. Interface-driven thermal rectification in nanoscale systems. *Phys. Rev. Mater.* **2018**, *2*, 113001.
(31) Jiang, P.; Hu, S.; Ouyang, Y.; Ren, W.; Yu, C.; Zhang, Z.; Chen, J. Remarkable thermal rectification in pristine and symmetric monolayer graphene enabled by asymmetric thermal contact. *J. Appl. Phys.* **2020**, *127*, 235101.
(32) Melis, C.; Barbarino, G.; Colombo, L. Exploiting hydrogenation for thermal rectification in graphene nanoribbons. *Phys. Rev. B: Condens. Matter Mater. Phys.* **2015**, *92*, 245408.
(33) Wang, H.; Hu, S.; Takahashi, K.; Zhang, X.; Takamatsu, H.; Chen, J. Experimental study of thermal rectification in suspended monolayer graphene. *Nat. Commun.* **2017**, *8*, 15843.
(34) Nobakht, A. Y.; Gandomi, Y. A.; Wang, J.; Bowman, M. H.; Marable, D. C.; Garrison, B. E.; Kim, D.; Shin, S. Thermal rectification via asymmetric structural defects in graphene. *Carbon* **2018**, *132*, 565−572.
(35) Kobayashi, W.; Teraoka, Y.; Terasaki, I. An oxide thermal rectifier. *Appl. Phys. Lett.* **2009**, *95*, 171905.
(36) Takeuchi, T.; Goto, H.; Nakayama, R.-S.; Terazawa, Y.-I.; Ogawa, K.; Yamamoto, A.; Itoh, T.; Mikami, M. Improvement in rectification ratio of an Al-based bulk thermal rectifier working at high temperatures. *J. Appl. Phys.* **2012**, *111*, 093517.
(37) Kobayashi, W. Thermal-rectification coefficients in solid-state thermal rectifiers. *Phys. Rev. E* **2020**, *102*, 032142.
(38) Wang, J.-X.; Birbarah, P.; Docimo, D.; Yang, T.; Alleyne, A. G.; Miljkovic, N. Nanostructured jumping-droplet thermal rectifier. *Phys. Rev. E* **2021**, *103*, 023110.
(39) Pop, E.; Varshney, V.; Roy, A. K. Thermal properties of graphene: Fundamentals and applications. *MRS Bull.* **2012**, *37*, 1273−1281.
(40) Chen, S.; Wu, Q.; Mishra, C.; Kang, J.; Zhang, H.; Cho, K.; Cai, W.; Balandin, A. A.; Ruoff, R. S. Thermal conductivity of isotopically modified graphene. *Nat. Mater.* **2012**, *11*, 203−207.
(41) Seol, J. H.; Jo, I.; Moore, A. L.; Lindsay, L.; Aitken, Z. H.; Pettes, M. T.; Li, X. S.; Yao, Z.; Huang, R.; Broido, D.; Mingo, N.; Ruoff, R. S.; Shi, L. Two-dimensional phonon transport in supported graphene. *Science* **2010**, *328*, 213−216.
(42) Liao, A. D.; Wu, J. Z.; Wang, X.; Tahy, K.; Jena, D.; Dai, H.; Pop, E. Thermally limited current carrying ability of graphene nanoribbons. *Phys. Rev. Lett.* **2011**, *106*, 256801.
(43) Haskins, J.; Kınacı, A.; Sevik, C.; Sevinçli, H.; Cuniberti, G.; Çağın, T. Control of thermal and electronic transport in defect-engineered graphene nanoribbons. *ACS Nano* **2011**, *5*, 3779−3787.
(44) Zhang, H.; Lee, G.; Cho, K. Thermal transport in graphene and effects of vacancy defects. *Phys. Rev. B: Condens. Matter Mater. Phys.* **2011**, *84*, 115460.
(45) Péraud, J.-P. M.; Hadjiconstantinou, N. G. Efficient simulation of multidimensional phonon transport using energy-based variance-reduced Monte Carlo formulations. *Phys. Rev. B: Condens. Matter Mater. Phys.* **2011**, *84*, 205331.
(46) Arora, A.; Hori, T.; Shiga, T.; Shiomi, J. Thermal rectification in restructured graphene with locally modulated temperature dependence of thermal conductivity. *Phys. Rev. B* **2017**, *96*, 165419.
(47) Peraud, J.-P. M.; Landon, C. D.; Hadjiconstantinou, N. G. Monte Carlo methods for solving the Boltzmann transport equation. *Annu. Rev. Heat Transfer* **2014**, *17*, 205−265.
(48) Péraud, J.-P. M.; Hadjiconstantinou, N. G. An alternative approach to efficient simulation of micro-nanoscale phonon transport. *Appl. Phys. Lett.* **2012**, *101*, 153114.
(49) Radtke, G. A.; Péraud, J.-P. M.; Hadjiconstantinou, N. G. On efficient simulations of multiscale kinetic transport. *Philos. Trans. R. Soc., A* **2013**, *371*, 20120182.
(50) Homolle, T. M. M.; Hadjiconstantinou, N. G. A low-variance deviational simulation Monte Carlo for the Boltzmann equation. *J. Comput. Phys.* **2007**, *226*, 2341−2358.
(51) Wang, Y.; Shang, S.-L.; Fang, H.; Liu, Z.-K.; Chen, L.-Q. First-principles calculations of lattice dynamics and thermal properties of polar solids. *npj Comput. Mater.* **2016**, *2*, 16006.
(52) Cooke, J. R.; Lukes, J. R. An implicit spin lattice dynamics integrator in LAMMPS. *Comput. Phys. Commun.* **2022**, *271*, 108203.
(53) Barbalinardo, G.; Chen, Z.; Lundgren, N. W.; Donadio, D. Efficient anharmonic lattice dynamics calculations of thermal transport in crystalline and disordered solids. *J. Appl. Phys.* **2020**, *128*, 135104.
(54) Hanus, R.; Gurunathan, R.; Lindsay, L.; Agne, M. T.; Shi, J.; Graham, S.; Snyder, G. J. Thermal transport in defective and disordered materials. *Appl. Phys. Rev.* **2021**, *8*, 031311.
(55) Swartz, E. T.; Pohl, R. O. Thermal boundary resistance. *Rev. Mod. Phys.* **1989**, *61*, 605−668.
(56) Yang, B.; Chen, G. Partially coherent phonon heat conduction in superlattices. *Phys. Rev. B: Condens. Matter Mater. Phys.* **2003**, *67*, 195311.
(57) Marucha, C.; Mucha, J.; Rafałowicz, J. Heat flow rectification in inhomogeneous GaAs. *Phys. Status Solidi A* **1975**, *31*, 269−273.
(58) Hudson, P. R. W. Heat flow rectification. *Phys. Status Solidi A* **1976**, *37*, 93−96.
(59) Miller, J.; Jang, W.; Dames, C. Thermal rectification by ballistic phonons. *ASME 2008 3rd Energy Nanotechnology International Conference collocated with the Heat Transfer, Fluids Engineering, and Energy Sustainability Conferences*; ASME: Jacksonville, Florida, United States, 2008.
(60) Dames, C. Solid-state thermal rectification with existing bulk materials. *J. Heat Transfer* **2009**, *131*, 061301.
(61) Fthenakis, Z. G.; Zhu, Z.; Tománek, D. Effect of structural defects on the thermal conductivity of graphene: From point to line defects to haeckelites. *Phys. Rev. B: Condens. Matter Mater. Phys.* **2014**, *89*, 125421.
(62) Esfahani, M. N.; Jabbari, M.; Xu, Y.; Soutis, C. Effect of nanoscale defects on the thermal conductivity of graphene. *Mater. Today Commun.* **2021**, *26*, 101856.
(63) Wang, Z.; Alaniz, J. E.; Jang, W.; Garay, J. E.; Dames, C. Thermal conductivity of nanocrystalline silicon: Importance of grain size and frequency-dependent mean free paths. *Nano Lett.* **2011**, *11*, 2206−2213.
(64) Shiga, T.; Shiomi, J. Modulating temperature dependence of thermal conductivity by nanostructuring. *Jpn. J. Appl. Phys.* **2018**, *57*, 120312.
(65) Balandin, A. A.; Ghosh, S.; Nika, D. L.; Pokatilov, E. P. Thermal conduction in suspended graphene layers. *Fullerenes, Nanotubes Carbon Nanostruct* **2010**, *18*, 474−486.
(66) Nika, D. L.; Ghosh, S.; Pokatilov, E. P.; Balandin, A. A. Lattice thermal conductivity of graphene flakes: Comparison with bulk graphite. *Appl. Phys. Lett.* **2009**, *94*, 203103.

https://doi.org/10.1021/acsomega.2c02041
ACS Omega 2022, 7, 28030−28040